

Towards Stabilized and Efficient Diffusion Transformers through Long-Skip-Connections with Spectral Constraints

Guanjie Chen^{1,2,6*} Xinyu Zhao^{3*} Yucheng Zhou⁴ Xiaoye Qu^{2,5} Tianlong Chen^{3†} Yu Cheng^{6†}

¹Shanghai Jiao Tong University ²Shanghai Artificial Intelligence Laboratory

³The University of North Carolina at Chapel Hill ⁴SKL-IOTSC, CIS, University of Macau

⁵Huazhong University of Science and Technology ⁶The Chinese University of Hong Kong

chenguangjie@sjtu.edu.cn, xinyu@cs.unc.edu

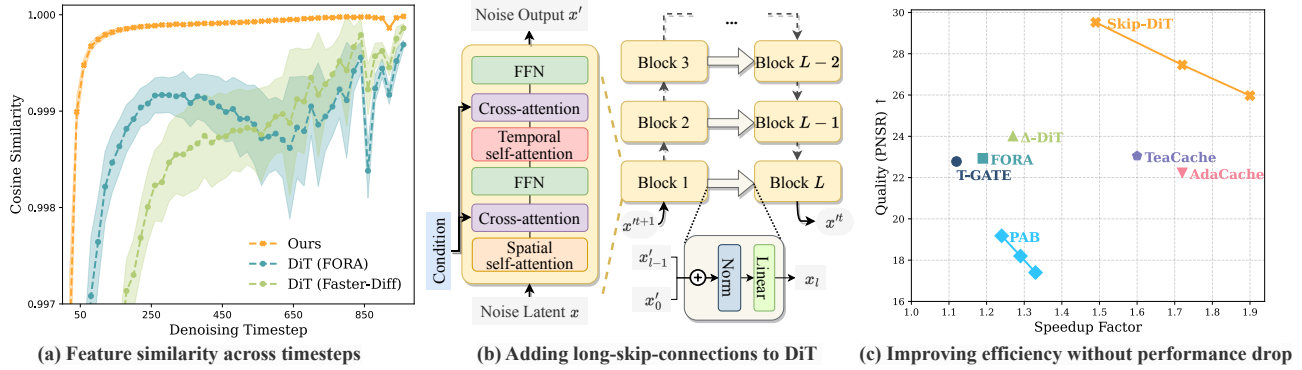


Figure 1. (a) Feature similarities between standard and cache-accelerated outputs in vanilla DiT (caching with FORA [30] and Faster-Diff [13]) and our proposed Skip-DiT. Skip-DiT presents consistently higher feature similarity, demonstrating superior stability after caching. (b) Illustration of Skip-DiT that modifies vanilla DiT models using long-skip-connection to connect shallow and deep DiT blocks. Dashed arrows indicate paths where computation can be skipped in cached inference. (c) Comparison of video generation quality (PNSR) and inference speedup of different DiT caching methods. Skip-DiT maintains higher generation quality even at greater speedup factors.

Abstract

Diffusion Transformers (DiT) have emerged as a powerful architecture for image and video generation, offering superior quality and scalability. However, their practical application suffers from inherent dynamic feature instability, leading to error amplification during cached inference. Through systematic analysis, we identify the absence of long-range feature preservation mechanisms as the root cause of unstable feature propagation and perturbation sensitivity. To this end, we propose Skip-DiT, an image and video generative DiT variant enhanced with Long-Skip-Connections (LSCs) - the key efficiency component in U-Nets. Theoretical spectral norm and visualization analysis demonstrate how LSCs stabilize feature dynamics. Skip-DiT architecture and its stabilized dynamic feature enable an efficient static caching mechanism that reuses deep features across timesteps while updating shallow components. Extensive experiments across the image and video generation tasks demonstrate that Skip-DiT achieves: (1) $4.4 \times$ training

acceleration and faster convergence, (2) $1.5 - 2 \times$ inference acceleration with negligible quality loss and high fidelity to the original output, outperforming existing DiT caching methods across various quantitative metrics. Our findings establish Long-Skip-Connections as critical architectural components for stable and efficient diffusion transformers. Codes are provided in the URL¹.

1. Introduction

Diffusion models [3, 8, 24, 51] have emerged as the de-facto solution for visual generation, owing to their high fidelity outputs and ability to incorporate various conditioning signals, particularly natural language. Classical diffusion models typically adopt U-Net [27] as their denoising backbone. Recently, Diffusion Transformers (DiT) [4, 23] introduce an alternative architecture to replace traditional convolutional

¹<https://github.com/OpenSparseLLMs/Skip-DiT>

*Equal Contribution.

†Corresponding Authors.

networks with Vision Transformers, offering enhanced scalability potential. While initially designed for image generation, DiT has demonstrated remarkable effectiveness when extended to video generation tasks [14, 18, 25]. Despite these advances, DiT still faces challenges in practical deployment due to its slow convergence rates [20, 44, 52] and substantial inference time requirements, posing significant constraints on training efficiency and real-time applications.

Numerous approaches have been proposed to improve the efficiency of diffusion models, including reduced sampling techniques [33], distillation methods [29, 45], and quantization strategies [5]. Among these approaches, caching has emerged as one of the most effective strategies for enhancing inference efficiency, owing to its low computational cost while maintaining high fidelity and similarity to the original models through efficient feature reuse [6, 11, 16, 30, 49, 53]. However, existing caching methods in DiT still face challenges in visual generation. DiT architecture exhibits significant sample-wise variation in caching function responses, requiring adaptive per-sample hyperparameter tuning and introducing computational overhead [11, 16]. Besides, current caching methods still yield suboptimal generative results with visible artifacts when cached with larger intervals [6, 11, 30, 53], suggesting error amplification in DiT’s transformer blocks. Besides, the training efficiency gap further compounds these challenges. DiT is shown to converge more slowly in training [44, 52], and the reasons remain unexplained from architectural perspectives.

DiT efficiency is hindered by the above challenges, but U-Net-based diffusion models can leverage their Long-Skip-Connections (LSCs) to extend cache intervals without complex timestep scheduling or severe performance degradation [13, 17]. The LSCs not only make caching stable and robust during inference, but they have also been proven as the key factor for stabilizing training and accelerating convergence for U-Net-based diffusion models [9]. These observations lead to our core research question:

(Q) What are the architectural root causes of feature instability and inefficiency in DiT, and to what extent can Long-Skip-Connections mitigate these issues while preserving generation quality?

In this study, we systematically analyze the feature distribution in DiT: ① We conduct a preliminary experiment that incorporates Long-Skip-Connections (LSCs) with DiT, and visualize the dynamic features of DiT with and without LSCs by adding perturbations in parameters and model inputs, the feature similarity landscape and plots validate the instability of vanilla DiT (w/o LSCs), which we formally characterize as *Dynamic Feature Instability*, indicating an uncontrolled spectral norm that affects both statistical stability, model robustness, and convergence rate. ② We then theoretically prove the superior stability and robustness of DiT with LSCs

over vanilla DiT via spectral analysis

To this end, we propose the **Long-Skip-Connected-DiT**, namely **Skip-DiT**, a DiT architecture that employs spectral constraints—limiting the maximum singular value of weight matrices to ensure stable gradient flow and reduced sensitivity to perturbations. By incorporating these constraints through LSCs, our approach provides theoretical feature stability guarantees and enhanced efficiency in both training and inference, validated through quantitative experiments and visual analysis. The LSCs also enable output caching of stabilized features from deep blocks, requiring the computation of only shallow blocks during inference at statically chosen caching timesteps.

To evaluate our proposed **Skip-DiT**, we conduct extensive experiments across 3 DiT backbones, assess training performance on 6 models, and inference efficiency on 7 visual generation tasks, spanning both class and text conditional image/video generation. **Skip-DiT** achieves superior training efficiency while consistently outperforming both standard baselines and prior caching methods in qualitative and quantitative evaluations. To summarize, we claim the following contribution of this work:

- Through theoretical analysis and comprehensive visualization, we identify *Dynamic Feature Instability* as a fundamental root cause that impairs DiT training efficiency and hinders effective inference acceleration.
- We introduce **Skip-DiT**, an enhanced DiT architecture incorporating LSCs between shallow and deep transformer blocks. We provide theoretical guarantees for feature stability through spectral norm analysis and enable efficient feature caching at strategically selected timesteps.
- Results of substantial training and inference speedup and nearly undamaged generation quality consistently endorse the effectiveness of **Skip-DiT**. For example, compared to vanilla DiT, **Skip-DiT** achieves up to 4.4× training acceleration with even better generation quality. When compared to state-of-the-art DiT caching techniques, **Skip-DiT** delivers 1.5-2× additional speedup while maintaining superior output fidelity.

2. Related Works

Transformer-based Diffusion Models The diffusion model has become the dominating architecture for image and video generation, whose main idea is iterative generate high-fidelity images or video frames from noise [26]. Early diffusion models mainly employ U-Net as their denoising backbone [3, 24]. However, U-Net architectures struggle to model long-range dependencies due to the local nature of convolutions. Researchers proposing diffusion transformer model (DiT) for image generation [2, 4, 23]. Recent years have witnessed a significant growth in studies of video DiT. Proprietary DiT such as Sora [20] and Movie-Gen [25] show impressive generation quality, also evidenced

by open-sourced implementation [12, 54]. Latte decomposes the spatial and temporal dimensions into four efficient variants for handling video tokens, allowing effective modeling of the substantial number of tokens extracted from videos in the latent space [18]. CogvideoX adds a 3D VAE combined with an expert transformer using adaptive LayerNorm, which enables the generation of longer, high-resolution videos [43].

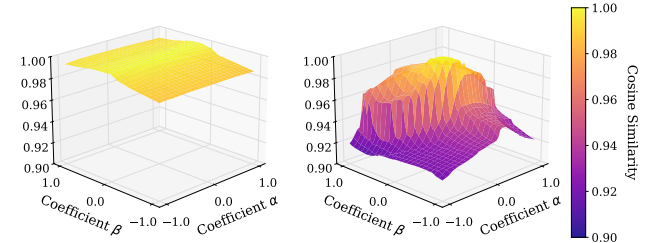
Diffusion Acceleration with Feature Caching Since the diffusion model involves iterative denoising, caching features across time-steps, model layers, and modules has been found an effective way to save inference computation costs. For U-Net Diffusion, DeepCache [17] and FRDiff [32] exploit temporal redundancy by reusing features across adjacent denoising steps. While other works take a more structured approach by analyzing and caching specific architectural components—Faster Diffusion [13] specifically targets encoder feature reuse while enabling parallel decoder computation, and Block Caching [41] introduces automated caching schedules for different network blocks based on their temporal stability patterns. Recently, cache-based acceleration has also been applied to DiT. PAB [53] introduces a pyramid broadcasting strategy for attention outputs. Δ -DiT [6] proposes adaptive caching of different DiT blocks based on their roles in a generation–rear blocks during early sampling for details and front blocks during later stages for outlines. T-Gate [50] identifies a natural two-stage inference process, enabling the caching and reuse of text-oriented semantic features after the initial semantics-planning stage. To deal with the sample-wise variation in DiT, adaptive caching methods like AdaCache [11] and TeaCache [16] are proposed to predict the feature distribution according to the input.

Long Skip Connections in DiT Although previous works like HunyuanDiT [14] and U-DiT [37] have incorporated Long Skip Connections (LSCs) into DiTs, a systematic analysis of their functional role has been absent. Our work provides this analysis, highlighting the distinct advantages of our implementation. We contrast our approach with U-DiT [37], which employs token and feature downsampling primarily for complexity reduction. Instead, our method uses deep-to-shallow LSCs to enhance the model’s spectral properties, boosting feature stability and training convergence. These connections preserve original dimensions, enabling an effective statistic-cached inference by mixing recomputed and cached features. A key advantage is that our method retains the native DiT block structure, permitting conversion from pre-trained models through continued training, unlike U-DiT which necessitates retraining from scratch.

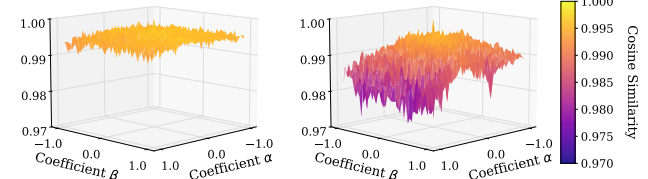
3. Methodology

3.1. Preliminaries

Diffusion model The concept of diffusion models mirrors particle dispersion physics, where particles spread out with



(a) Feature similarity landscape on class-to-image task.



(b) Feature similarity landscape on text-to-video task.

Figure 2. Feature stability comparison between Skip-DiT (left) and vanilla DiT (right) on class-to-image (DiT-XL) and text-to-video (Latte) generation. We inject perturbations δ (magnitudes α) and η (magnitudes β), normalized with specific coefficients ($\epsilon = 1e^{-3}$ for DiT-XL and $2e^{-2}$ for Latte), then measure the similarity between the standard and perturbed features.

random motion. It involves forward and backward diffusion. The forward phase adds noise to data across T timesteps. Starting from data $\mathbf{x}_0 \sim q(\mathbf{x})$, noise is added to the data at each timestep $t \in \{1 \dots T\}$.

$$\mathbf{x}_t = \sqrt{\alpha_t} \mathbf{x}_{t-1} + \sqrt{1 - \alpha_t} \epsilon_{t-1} \quad (1)$$

where α determines noise level while $\epsilon \sim \mathcal{N}(0, \mathbf{I})$ represents Gaussian noise. The data \mathbf{x}_t becomes increasingly noisy with time, reaching $\mathcal{N}(0, \mathbf{I})$ at $t = T$. Reverse diffusion then reconstructs the original data as follows, where μ_θ and Σ_θ refer to the learnable mean and covariance:

$$p_\theta(\mathbf{x}_{t-1} | \mathbf{x}_t) = \mathcal{N}(\mathbf{x}_{t-1}; \mu_\theta(\mathbf{x}_t, t), \Sigma_\theta(\mathbf{x}_t, t)), \quad (2)$$

3.2. Dynamic Feature Instability in DiT

DiT models are known to suffer from low training efficiency [52] and unstable feature distributions during inference [11, 16], posing significant challenges for acceleration and their application in interleaved reasoning [35, 36]. This contrasts sharply with U-Net [27] architectures where Long-Skip-Connections (LSCs) enhance training stability and efficiency [9], and enable simple but reliable acceleration through feature reuse [13, 17]. To explore this architectural discrepancy, we integrate LSCs into DiT-XL [22] as in Figure 2 (b) and train from scratch as the preliminary experiment. Training settings is the same as in Section 4.1

Visualizing Feature Stability of DiT Let $\theta \in \mathbb{R}^d$ denote the original parameters of model $f(x; \theta)$. Given random

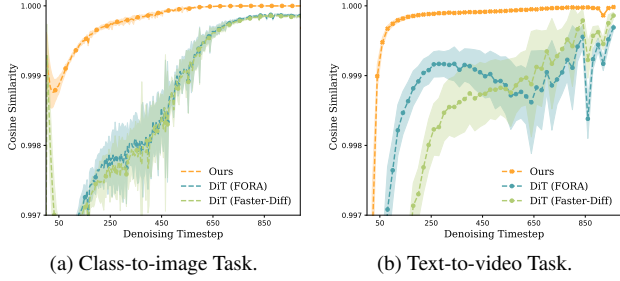


Figure 3. Comparison between standard and cache-accelerated outputs in vanilla DiT versus Skip-DiT, with Latte (text-to-video generation) and DiT-XL (class-to-image generation) serving as base architectures. Both mean and standard deviation across samples are shown. Vanilla DiT exhibits much higher sample variance.

perturbation vectors $\delta, \eta \in \mathbb{R}^d$, $\|\delta\| = \|\eta\| = \epsilon\|\theta\|$, with $0 < \epsilon < 1$ which is normalization coefficient. we construct perturbed parameters: $\theta' = \theta + \alpha\delta + \beta\eta$, where $\alpha, \beta \in \mathbb{R}$ control perturbation magnitudes. The feature stability landscape for 3D visualization is defined as:

$$L(\alpha, \beta) = \text{CosineSimilarity}(f(x; \theta), f(x; \theta')) \quad (3)$$

To visualize the feature stability across timesteps, we perturb the inputs with cached values, following the caching strategy of FORA[30] and FasterDiff[44], and we take cosine similarity to measure the distance with and without caching. Visualized results are illustrated in Figure 2(a) and 3(a).

Dynamic Feature Instability Our preliminary experiments and visualizations reveal that vanilla DiT models exhibit significant sensitivity to perturbations in both parameters and input features, with feature similarity across timesteps demonstrating considerable variability across different examples. These observations raise critical concerns regarding the stability of DiT models, particularly for training efficiency and inference acceleration. We formally define the instability of DiT as *Dynamic Feature Instability* (DFI). We preliminary attribute these issues to the uncontrolled spectral norm σ_{\max} of DiT’s Jacobians J^{vanilla} , which exponentially amplifies perturbations and destabilizes feature propagation. This aligns with findings in [46], where high spectral norms degrade model robustness and generalization capacity by amplifying input sensitivities, and mirrors the instability patterns observed in visual generative GAN training [19] without spectral normalization.

Training Convergence Comparison To validate the theoretical convergence rate in real implementations, we extend preliminary experiments recording the relationship between training steps and performance and FID[21] on ImageNet[7]. Both DiT models with/without LSCs are trained from scratch under identical settings. Results are revealed in Figure 4. The accelerated convergence of DiT w/ LSCs observed in practical training demonstrates the training efficiency and model capability. This mirrors our theoretical analysis in

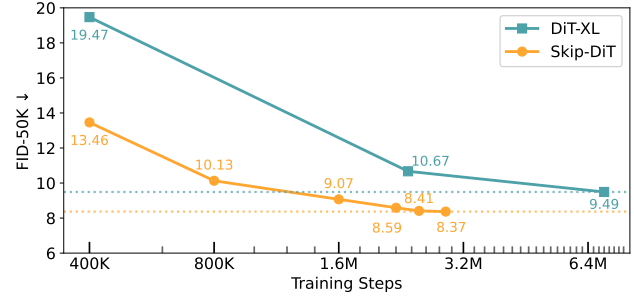


Figure 4. Training efficiency comparison between Skip-DiT and DiT-XL. Skip-DiT achieves superior FID-50K score on ImageNet at 1.6M training steps (vs. DiT-XL’s 7M steps) and converges faster at 2.9M steps. Both models are evaluated on FID-50K under identical settings (no classifier-free guidance, $\text{cfg}=1$).

Theorem 1, confirming that the spectral norm is effectively controlled with LSCs during training.

3.3. Integrating Long-Skip-Connection into DiT

To detail the DiT with Long-Skip-Connections(LSCs), we connect the shallow blocks to deep blocks with LSCs in DiT, named as Skip-DiT. Let \mathbf{x} denote the input noise embedding, and \mathbf{x}'_l represents the output at the l -th layer of Skip-DiT. The architecture consists of L sequential DiT blocks with LSCs. Each DiT block $\mathcal{F}_{\text{DiT}}^l$ at block l processes the features as $\mathbf{x}' = \mathcal{F}_{\text{DiT}}^l(\mathbf{x})$. The i -th skip branch ($i \in \{1 \dots L//2\}$) connects i -th block to $(L+1-i)$ -th block, which can be denoted as $\mathcal{F}_{\text{Skip}}^i(\cdot, \cdot)$. Given output \mathbf{x}'_i from the start of the skip branch and \mathbf{x}'_{l-1} from the previous layer, the skip branch aggregates them to the input to l -th block as:

$$\mathbf{x}_l = \mathcal{F}_{\text{skip}}^i(\mathbf{x}'_i, \mathbf{x}'_{l-1}) = \text{Linear}(\text{Norm}(\mathbf{x}'_i \oplus \mathbf{x}'_{l-1})) \quad (4)$$

where \oplus denotes concatenation, Norm represents the layer normalization, and Linear is a fully-connected layer. Each skip connection creates a shortcut path that helps preserve and process information from earlier layers, enabling better gradient flow and feature reuse throughout the network.

3.4. Spectral Analysis of Skip-DiT

Consider an ideal denoising diffusion transformer M with L identical blocks, where the denoising capability induces the following fundamental properties:

- **Noise Reduction Invariance:** Each transformer block \mathcal{T}_l strictly reduces noise magnitude of input h . This directly implies the Jacobian spectral norm (σ_{\max}) constraint:

$$\sigma_{\max} \left(\frac{\partial \mathcal{T}_l}{\partial h} \right) \triangleq \gamma_l < 1 \quad (5)$$

- **Transformer Blocks Homogeneity:** Identical noise reduction ratio across layers $\gamma_l = \gamma$, $\forall l \in \{1, \dots, L\}$. Thus, the complete model satisfies

$$\sigma_{\max}(M) = \prod_{l=1}^L \gamma = \gamma^L \ll 1 \quad (6)$$

Theorem 1. *The spectral norm of the Jacobian matrix of DiT with Long-Skip-Connections is controlled more tightly than that of Vanilla DiT M , making the Skip-DiT model more robust, numerically stable, and capable of converging faster.*

Proof. Define layer transformations for $L/2 < l \leq L$ and their Jacobian matrices, where \mathcal{T} denotes the Transformer block and $0 < \alpha < 1$ denotes normalized concatenation:

$$h_{l+1}^{\text{vanilla}} = \mathcal{T}(h_l^{\text{vanilla}}), h_{l+1}^{\text{skip}} = (1 - \alpha) \cdot \mathcal{T}(h_l^{\text{skip}}) + \alpha \cdot h_{L-l}^{\text{skip}}.$$

The corresponding Jacobian matrices J are:

$$J_l^{\text{vanilla}} = \frac{\partial \mathcal{T}(h_l)}{\partial h_l}, J_l^{\text{skip}} = (1 - \alpha) \cdot \frac{\partial \mathcal{T}(h_l)}{\partial h_l} + \alpha \cdot \frac{\partial h_{L-l}}{\partial h_l}.$$

Given $\gamma < 1$ and $2l - L \geq 1$ for $l \geq L/2$, the layer wise spectral norms σ_{\max} of M_{vanilla} and M_{skip} satisfy:

$$\sigma_{\max}(J_l^{\text{skip}}) \leq (1 - \alpha)\gamma + \alpha\gamma^{2l-L} < \gamma = \sigma_{\max}(J_l^{\text{vanilla}})$$

For the full model Jacobian $J = \prod_{l=1}^L J_l$, the σ_{\max} satisfy:

$$\sigma_{\max}(J^{\text{skip}}) < \prod_{l=0}^{L-1} \gamma = \gamma^L = \sigma_{\max}(J^{\text{vanilla}}). \quad (7)$$

This spectral norm reduction attenuates perturbation growth through $\|\Delta h_L\| \leq (\sigma_{\max}(J))^L \|\Delta h_0\|$, stabilizes gradient flow via $\|\nabla_{\theta} \mathcal{L}\| \leq \sigma_{\max}(J) \|\nabla_{h_L} \mathcal{L}\|$. This theoretical analysis aligns with our findings in Section 3.2, where Skip-DiT is proven to be more feature stable and training efficient through visualizations and preliminary experiments.

3.5. Cached Inference Mechanism

The feature stability and robustness in Skip-DiT enables effective reuse of intermediate features across timesteps during denoising. To quantify this advantage, we analyze the similarity of transformer block outputs with versus without caching in both vanilla DiT and Skip-DiT.

Caching Strategy for Skip-DiT For Skip-DiT, we implement a hybrid caching strategy combining skip-connection-based block skipping from DeepCache [17], phased denoising strategy [13, 50], and errors accumulation guidance [11, 16]. As illustrated in Figure 3, our guidance mechanism is informed by a static error record \mathcal{R} , which is pre-computed by averaging historical prediction errors. To optimize the caching process, we also identify an optimal dynamic phase, \mathcal{P} , through static feature analysis. The choice \mathcal{P} is substantiated by our ablation study in Table 5 and visualization in Figure 5. The complete inference procedure is formally outlined in Algorithm 1.

Visualizing Caching Stability As visualized in Figure 3, Skip-DiT exhibits significantly higher feature similarity and smaller variance among examples compared to vanilla DiT, which employs FORA [30] and FasterDiffusion designed for DiT models. This demonstrates superior stability for cached inference. We attribute this to the inherent feature stabilization and enhanced robustness. The latter can be theoretically grounded on M defined in Section 3.4:

Theorem 2. *Under feature reuse with interval τ , Skip-DiT achieves tighter perturbation bounds than Vanilla DiT, enabling larger allowable reuse intervals while maintaining error tolerance ϵ_{\max} .*

Proof. Let h_t be the reused feature with error ϵ_t , δ the perturbation bound per step, x the input, and θ the model parameters. Through the differential mean-value theorem and error propagation:

$$\epsilon_{t+1} = \|h_{t+1} - h_t\| \leq \text{Lip}(M)\epsilon_t + \delta$$

From Theorem 1, the Lipschitz constants and perturbation bounds satisfy: $\text{Lip}(M_{\text{skip}}) < \text{Lip}(M_{\text{vanilla}})$ and $\delta_{\text{skip}} < \delta_{\text{vanilla}}$. For T -step feature reuse, the cumulative error is:

$$\epsilon_T \leq \frac{\text{Lip}(M)^T - 1}{\text{Lip}(M) - 1} \delta \quad (8)$$

Considering the conditions above, the maximal interval τ satisfies: $\epsilon_{\tau}^{\text{skip}} = \epsilon_{\tau}^{\text{vanilla}} < \epsilon_{\max}$. Solving this yields $\tau_{\text{skip}} > \tau_{\text{vanilla}}$ under identical ϵ_{\max} , which demonstrate better robustness and tolerance to error of Skip-DiT.

4. Experiments

4.1. Implementation Details

Models To start with, we add LSCs in DiT-XL [22] on the class-to-image task to prove the training efficiency and feature stability of Skip-DiT. Then we employ Latte [18] as our base model in video generation and Hunyuan-DiT for text-to-image generation to further demonstrate the remarkable effectiveness of Skip-DiT and its caching efficiency. All DiT models are integrated with LSCs to evaluate the performance in both video and image generation tasks following the guidance in Section 3.3 and explore techniques for integrating LSCs into a pre-trained DiT model.

Datasets For the class-to-image task, Skip-DiT is trained on 256×256 ImageNet [7]. In the class-to-video task, Skip-DiT is trained on four datasets: FaceForensics [28], SkyTimelapse [42], UCF101 [34], and Taichi-HD [31]. Following the experimental settings in Latte, we extract 16-frame video clips from these datasets and resize all frames to a resolution of 256×256 . For the text-to-video task, the

Table 1. Class-to-video generation performance. The definition of the cache step n follows that in Table 2. For the UCF101 task, the scheduler is 50-steps-DDIM, while for the remaining tasks is 250-steps-DDPM. Latency and speedup are calculated on one A100 GPU. The notation $n = i$ represents cache interval N in Algorithm 1. We highlight Baseline DiT models in **grey**, and the best metrics in **bold**.

| Method | UCF101 | | FFS | | Sky | | Taichi | | FLOPs (T) | Latency (s) | Speedup |
|--------------------------------|---------------|--------------|--------------|-------------|--------------|--------------|---------------|------------------------|---------------|-------------|---------------|
| | FVD (↓) | FID (↓) | FVD (↓) | FID (↓) | FVD (↓) | FID (↓) | FVD (↓) | FID (↓) | | | |
| Latte | 155.22 | 22.97 | 28.88 | 5.36 | 49.46 | 11.51 | 166.84 | 11.57 | 278.63 | 9.90 | 1.00× |
| Δ-DiT | 161.62 | 25.33 | 25.80 | 4.46 | 51.70 | 11.67 | 188.39 | 12.09 | 226.10 | 8.09 | 1.22× |
| FORA | 160.52 | 23.52 | 27.23 | 4.64 | 52.90 | 11.96 | 198.56 | 13.68 | 240.26 | 9.00 | 1.10× |
| PAB ₂₃ | 213.50 | 30.96 | 58.15 | 5.94 | 96.97 | 16.38 | 274.90 | 16.05 | 233.87 | 7.63 | 1.30× |
| PAB ₃₅ | 1176.57 | 93.30 | 863.18 | 128.34 | 573.72 | 55.66 | 828.40 | 42.96 | 222.90 | 7.14 | 1.39× |
| Skip-DiT with Cached Inference | | | | | | | | | | | |
| original | 141.30 | 23.78 | 20.62 | 4.32 | 49.21 | 11.92 | 163.03 | 13.55 | 290.05 | 10.02 | 1.00× |
| $n = 2$ | 141.42 | 21.46 | 23.55 | 4.49 | 51.13 | 12.66 | 167.54 | 13.89 (0.34 ↑) | 180.68 | 6.40 | 1.56× |
| $n = 3$ | 137.98 | 19.93 | 26.76 | 4.75 | 54.17 | 13.11 | 179.43 | 14.53 | 145.87 | 5.24 | 1.91× |
| $n = 4$ | 143.00 | 19.03 | 30.19 | 5.18 | 57.36 | 13.77 | 188.44 | 14.38 | 125.99 | 4.57 | 2.19× |
| $n = 5$ | 145.39 | 18.72 | 35.52 | 5.86 | 62.92 | 14.18 | 209.38 | 15.20 | 121.02 | 4.35 | 2.30× |
| $n = 6$ | 151.77 | 18.78 | 42.41 | 6.42 | 68.96 | 15.16 | 208.04 | 15.78 | 111.07 | 4.12 | 2.43 × |

Algorithm 1 Skip-DiT with Cached Inference

Input Initial state \mathbf{x}^t , model \mathcal{F} , cache interval N , global error ϵ , static error records $\mathcal{R}(x_{t=1}^T)$, dynamic Phase \mathcal{P} .
Output Generated sequence $\{\mathbf{x}^t\}_{t=1}^T$

- 1: **Global Timestep t (Full Inference):**
- 2: $\mathbf{x}'^t \leftarrow \mathcal{F}^{L-1} \circ \dots \circ \mathcal{F}^1(\mathbf{x}^t)$
- 3: Cache feature: $\mathcal{C}_{L-1}^t \leftarrow \mathbf{x}'^t$
- 4: $\mathbf{x}^{t-1} = \mathcal{F}^L(\mathbf{x}^t)$
- 5: **for** $k = 1$ **to** $N - 1$ **do**
- 6: **Local Timestep $t - k$ (Cached Inference):**
- 7: $\mathbf{x}_1^{t-k} \leftarrow \mathcal{F}_{\text{DiT}}^1(\mathbf{x}^{t-k})$
- 8: $\mathbf{x}^{t-k} \leftarrow \mathcal{F}_{\text{DiT}}^L(\mathcal{F}_{\text{Skip}}^1(\mathbf{x}_1^{t-k}, \mathcal{C}_{L-1}^t))$
- 9: Maintain cache: $\mathcal{C}_{L-1}^t \leftarrow \mathcal{C}_{L-1}^t$
- 10: Accumulate error: $\epsilon \leftarrow \epsilon + \mathcal{R}(t - k)$
- 11: **if** $t - k - 1 \in \mathcal{P}$ **||** $\epsilon > \text{threshold}$ **then**
- 12: $\epsilon \leftarrow 0$; **Break**
- 13: **end if**
- 14: **end for**
- 15: $t \leftarrow t - k - 1$;
- 16: **Back to Full Inference until:** $t < 0$;

original Latte is trained on Webvid [1] and Vimeo [39], comprising approximately 330k text-video pairs in total. Considering that the resolution of Webvid is lower than 512×512, we only sample 330k text-video pairs from Vimeo for training, with a resolution of 512×512 and 16 frames.

Training Details In the class-to-image task, the model is initialized randomly and aligns all the training settings with DiT-XL. The detailed training settings can be found in the Appendix. For class-to-video tasks, we train all instances of Skip-DiT from scratch on all datasets. For text-to-video tasks, we propose a two-stage continual training strategy:

• **Skip-Connections training:** Latte with LSC is initialized

with the weights of the original Latte, and the weight of LSCs is initialized randomly. At this stage, only the LSCs are trained. It only takes one day on 8 H100 GPUs.

- **Overall training:** With LSCs Fully trained, all other parameters are unfrozen to perform overall training. At this stage, Skip-DiT rapidly recovers its generation capability within two days and can generate content comparable to the original Latte with an extra three days of training.

All our training experiments are conducted on 8 H100 GPUs, video-image joint training strategy proposed by Ma et al. [18] is employed to enhance training stability.

4.2. Results on Video Generation Tasks

Evaluation Details Following previous works [11, 16, 53] and Latte, we evaluate text-to-video models using VBench [10], Peak Signal-to-Noise Ratio (PSNR), Learned Perceptual Image Patch Similarity (LPIPS) [48], and Structural Similarity Index Measure (SSIM) [40]. VBench is a comprehensive benchmark suite comprising 16 evaluation dimensions. PSNR is a widely used metric for assessing the quality of image reconstruction, LPIPS measures feature distances extracted from pre-trained networks, and SSIM evaluates structural information differences. For class-to-image tasks, we evaluate the similarity between generated and real videos using Fréchet Video Distance (FVD) [38] and Fréchet Inception Distance (FID) [21], following the evaluation guidelines of StyleGAN-V [47].

Class-to-video Generation We compare the quantitative performance of Latte and Skip-DiT on four class-to-video tasks, as shown in Table 1. Skip-DiT consistently outperforms Latte in terms of FVD scores across all tasks while achieving comparable performance in FID scores, demonstrating its strong video generation capabilities. Furthermore, we observe that Skip-DiT with cached inference significantly outperforms other caching methods across most met-

Table 2. Text-to-video generation performance. Inference latency and flops are evaluated with 1 A100 GPU. The notation $n = i$ represents the cache interval N in Algorithm 1. Baseline DiT models are highlighted in **grey**, and the best metrics are emphasized in **bold**.

| Model | Method | VBench(%) \uparrow | PSNR \uparrow | LPIPS \downarrow | SSIM \uparrow | FLOPs (T) | Latency (s) | Speedup |
|----------|--------------------|------------------------------------|-----------------|--------------------|-----------------|---------------|--------------|--------------------------------|
| Latte | original | 76.14 | — | — | — | 1587.25 | 27.11 | 1.00 \times |
| | T-GATE | 75.68 ($\downarrow 0.46$) | 22.78 | 0.19 | 0.78 | 1470.72 | 24.15 | 1.12 \times |
| | FORA | 76.06 ($\downarrow 0.08$) | 22.93 | 0.14 | 0.79 | 1341.72 | 24.21 | 1.19 \times |
| | Δ -DiT | 76.06 ($\downarrow 0.08$) | 24.01 | 0.17 | 0.81 | 1274.36 | 21.40 | 1.27 \times |
| | PAB ₂₃₅ | 73.77 ($\downarrow 2.37$) | 19.18 | 0.27 | 0.66 | 1288.08 | 23.24 | 1.24 \times |
| | PAB ₃₄₇ | 71.11 ($\downarrow 5.03$) | 18.20 | 0.32 | 0.63 | 1239.35 | 22.23 | 1.29 \times |
| | PAB ₄₆₉ | 70.20 ($\downarrow 5.94$) | 17.40 | 0.35 | 0.60 | 1210.11 | 21.60 | 1.33 \times |
| | AdaCache | 76.07 ($\downarrow 0.07$) | 22.23 | 0.19 | 0.78 | 934.85 | 16.95 | 1.60 \times |
| Skip-DiT | TeaCache | 76.03 ($\downarrow 0.11$) | 23.05 | 0.17 | 0.80 | 862.52 | 15.75 | 1.72 \times |
| | original | 75.60 | — | — | — | 1648.13 | 28.72 | 1.00 \times |
| | 65% steps cached | | | | | | | |
| | $n = 2$ | 75.51 ($\downarrow 0.09$) | 29.52 | 0.06 | 0.89 | 1127.83 | 19.28 | 1.49 \times |
| | $n = 3$ | 75.26 ($\downarrow 0.34$) | 27.46 | 0.09 | 0.85 | 974.80 | 16.67 | 1.72 \times |
| | $n = 4$ | 74.73 ($\downarrow 0.87$) | 25.97 | 0.13 | 0.81 | 882.98 | 15.12 | 1.90 \times |
| | 75% steps cached | | | | | | | |
| | $n = 2$ | 75.36 ($\downarrow 0.24$) | 26.02 | 0.10 | 0.84 | 1066.62 | 18.25 | 1.57 \times |
| | $n = 3$ | 75.07 ($\downarrow 0.53$) | 22.85 | 0.18 | 0.76 | 852.38 | 14.88 | 1.93 \times |
| | $n = 4$ | 74.43 ($\downarrow 1.17$) | 22.08 | 0.22 | 0.73 | 760.56 | 13.03 | 2.20\times |

rics, incurring only an average loss of 2.37 in the FVD score and 0.27 in the FID score while achieving a 1.56 \times speedup.

Text-to-video Generation Table 2 presents evaluation results on text-to-video models. Videos are generated using the prompts of VBench [10], which is considered a more generalized benchmark [10, 53, 54]. Compared with the original Latte, Skip-DiT achieves a comparable VBench score (75.60 vs. 76.14) with only six days of continual pre-training on 330k training samples. To demonstrate the superiority of the cached inference of Skip-DiT, we evaluate two caching settings: caching at timesteps 700 \rightarrow 50 and 800 \rightarrow 50 (out of 1000 timesteps in total). In both settings, Skip-DiT achieves the highest speedup while maintaining superior scores in PSNR, LPIPS, and SSIM, with only a minor loss in VBench score.

4.3. Results on Image Generation Tasks

We extend Skip-DiT to the class-to-image task, where Skip-DiT exceeds DiT-XL with only around 23% of its training cost (1.6M training steps vs. 7M), and we choose the Skip-DiT trained with 2.9M steps for evaluation. Hunyuan-DiT [14] is a powerful text-to-image DiT model featuring LSCs. However, its skip connections have not been fully explored to accelerate generation. We first explore their impact and efficiency potential and integrate it with our caching mechanism without architectural modifications.

Evaluation Details To evaluate the generalization of the caching mechanism in Skip-DiT for text-to-image tasks, we use the zero-shot Fréchet Inception Distance (FID) on the MS-COCO [15] validation dataset by generating 30k images based on its prompts, following the guidelines of Hunyuan-

DiT. Additionally, we also employ Peak Signal-to-Noise Ratio (PSNR), Learned Perceptual Image Patch Similarity (LPIPS), and Structural Similarity Index Measure (SSIM) to evaluate similarity. For the class-to-image task, we evaluate models on ImageNet [7] by generating 50k images, and calculating evaluation metrics used in Peebles and Xie [22].

Evaluation Results Table 3 comprehensively compares Hunyuan-DiT and various caching methods. Notably, our caching mechanism achieves a 2.09 \times speedup without any degradation in FID or CLIP scores. Furthermore, it outperforms all other caching methods in terms of PSNR, LPIPS, and SSIM scores, consistently maintaining the highest performance even with a 1.96 \times speedup. These findings underscore the robustness and adaptability of our caching mechanism to image generation tasks. Additionally, the unusual improvement in FID and CLIP scores is due to: ① In HunyuanDiT’s standard evaluation pipeline, FID fluctuates due to zero-shot evaluation and resolution scaling (1024 \rightarrow 256) prior to evaluation. ② The CLIP score is fluctuating within a reasonable range (-0.16, 0.2). These fluctuations are also observed in Δ -DiT. The results on the class-to-image task shown in Table 4, Skip-DiT also achieve the least loss while maintaining higher speedup.

4.4. Ablation Studies

Identify Dynamic Phase for Better Caching After incorporating LSCs into DiT, we can statically choose the timesteps for caching with feature stability, thus we can identify the dynamic phase by caching similarity shown in Figure 3. However, previous work has observed that the denoising process is split into different phases in U-Net diffusion models by Zhang et al. [49] and Li et al. [13],

Table 3. Text-to-image generation performance. Latency and speedup are calculated on one A100 GPU. The notation $n = i$ represents cache interval N in Algorithm 1. We highlight baseline DiT models (without caching) in grey, and the best metrics in bold.

| Method | FID (↓) | CLIP (↑) | PSNR (↑) | LPIPS (↓) | SSIM (↑) | FLOPs (T) | Latency (s) | Speedup |
|--------------------------------|--------------|--------------|--------------|-------------|-------------|---------------|-------------|-------------|
| HunYuan-DiT | 32.64 | 30.51 | — | — | — | 514.02 | 18.69 | 1.00 |
| TGATE | 32.71 | 30.64 | 16.80 | 0.24 | 0.61 | 378.94 | 13.21 | 1.41 |
| Δ-Cache | 28.35 | 30.35 | 16.56 | 0.21 | 0.65 | 362.67 | 13.58 | 1.38 |
| FORA | 31.21 | 30.53 | 19.58 | 0.14 | 0.75 | 330.68 | 13.20 | 1.42 |
| Skip-DiT with Cached Inference | | | | | | | | |
| $n = 2$ | 31.30 | 30.52 | 22.09 | 0.10 | 0.84 | 348.24 | 12.76 | 1.46 |
| $n = 3$ | 29.53 | 30.55 | 21.25 | 0.11 | 0.81 | 299.48 | 10.91 | 1.71 |
| $n = 4$ | 27.49 | 30.55 | 20.55 | 0.13 | 0.78 | 270.22 | 10.02 | 1.87 |
| $n = 5$ | 28.37 | 30.56 | 19.94 | 0.14 | 0.76 | 260.47 | 9.51 | 1.96 |
| $n = 6$ | 27.21 | 30.71 | 19.18 | 0.18 | 0.70 | 240.96 | 8.96 | 2.09 |

Table 4. Class-to-image generation performance. Speedups are calculated on an H100 GPU with a sample batch size of 8.

| Methods | FID ↓ | sFID ↓ | IS ↑ | Precision % | Recall % | Speedup |
|--------------------------------|-------------|-------------|---------------|--------------|--------------|--------------|
| DiT-XL | | | | | | |
| original | 2.30 | 4.71 | 276.26 | 82.68 | 57.65 | 1.00× |
| FORA | 2.45 | 5.44 | 265.94 | 81.21 | 58.36 | 1.57× |
| Delta-DiT | 2.47 | 5.61 | 265.33 | 81.05 | 58.83 | 1.45× |
| Skip-DiT with Cached Inference | | | | | | |
| original | 2.29 | 4.58 | 281.81 | 82.88 | 57.53 | 1.00× |
| $n = 2$ | 2.31 | 4.76 | 277.51 | 82.52 | 58.06 | 1.46× |
| $n = 3$ | 2.40 | 4.98 | 272.05 | 82.14 | 57.86 | 1.73× |
| $n = 4$ | 2.54 | 5.31 | 267.34 | 81.60 | 58.31 | 1.93× |

Table 5. Ablation study on different timestep ranges for caching. Total timesteps is 1000. Caching is performed at *caching timesteps*.

| Caching Timestep | VBench (%) ↑ | PSNR ↑ | LPIPS ↓ | SSIM ↑ |
|------------------|--------------|--------------|-------------|-------------|
| 700→50 | 75.51 | 29.52 | 0.06 | 0.89 |
| 950→300 | 75.48 | 20.58 | 0.23 | 0.73 |
| 800→50 | 75.36 | 26.02 | 0.10 | 0.84 |
| 900→50 | 75.24 | 22.13 | 0.19 | 0.76 |

highlighting the hidden dynamic phases which may lead to better performance. A heat map visualizing inner feature dynamics within blocks is shown in Figure 5, and significant changes are observed in the early denoising phase. In Table 5, we further validate this observation: under equivalent throughput, caching in the later timesteps (700→50), outperforms caching in the earlier timesteps (950→300) significantly. Additionally, we segmented the rapidly changing timesteps and experimented with additional caching ranges. All of these results show that increasing the ratio of the former phase significantly improves caching performance.

Compatibility of Skip-DiT As shown in Table 6, we extend the other text-to-video DiT caching methods to Skip-DiT and observe slight performance improvements. Taking PAB [53] as an example, it loses 1.15% less in VBench and achieves noticeably better PSNR and SSIM scores on Skip-DiT, demonstrating the compatibility of Skip-DiT, and that the stable features in Skip-DiT enhance the model robustness and caching efficiency.

Figure 5. The feature dynamics of Latte with LSCs. Differences in features at the same layers across timesteps are evaluated.

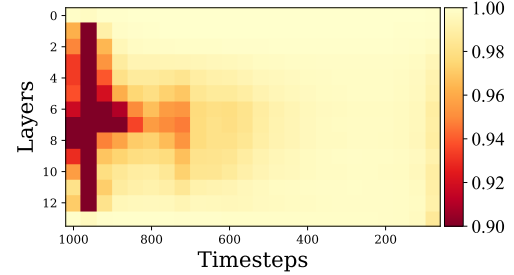


Table 6. Compatibility of Skip-DiT with other caching methods. Obvious improvements can be seen especially in PAB.

| Method | ΔVBench (%) ↓ | PSNR ↑ | LPIPS ↓ | SSIM ↑ |
|--------------------|---------------|--------------|-------------|-------------|
| T-GATE | 0.44 | 24.09 | 0.16 | 0.78 |
| Δ-DiT | 0.12 | 22.64 | 0.17 | 0.79 |
| FORA | 0.22 | 23.26 | 0.16 | 0.79 |
| PAB ₂₃₅ | 1.81 | 19.92 | 0.29 | 0.68 |
| PAB ₃₄₇ | 3.52 | 18.98 | 0.34 | 0.65 |
| PAB ₄₆₉ | 3.96 | 18.02 | 0.37 | 0.62 |

5. Conclusion

In this work, we identify the *Dynamic Feature Instability* in vanilla DiT models and introduce Skip-DiT, a Long-Skip-Connections enhanced DiT model to produce more stable features and build training and inference-efficient diffusion transformers. We designed a simple, static, but more efficient caching mechanism for Skip-DiT to improve inference efficiency in video and image generation tasks. By improving the stability of dynamic features, Skip-DiT unlocks the potential to cache most blocks while maintaining high generation quality. In addition, we guarantee stability and efficiency with theoretical analysis from the perspective of the spectral norm and visualizations. Furthermore, we identify the dynamic phase of Skip-DiT for a better caching strategy, demonstrating the effectiveness of caching. We also show that Skip-DiT is compatible with other caching methods, further extending its applicability. Overall, we believe that Skip-DiT provides a simple yet powerful foundation for advancing future research and applications.

Acknowledgement

During this project, Guanjie Chen is supported by Shanghai Artificial Intelligence Laboratory.

References

- [1] Max Bain, Arsha Nagrani, GÜl Varol, and Andrew Zisserman. Frozen in time: A joint video and image encoder for end-to-end retrieval. In *Proceedings of the IEEE/CVF international conference on computer vision*, pages 1728–1738, 2021. 6
- [2] Fan Bao, Shen Nie, Kaiwen Xue, Yue Cao, Chongxuan Li, Hang Su, and Jun Zhu. All are worth words: A vit backbone for diffusion models. *2023 IEEE/CVF Conference on Computer Vision and Pattern Recognition (CVPR)*, pages 22669–22679, 2022. 2
- [3] James Betker, Gabriel Goh, Li Jing, † TimBrooks, Jianfeng Wang, Linjie Li, † LongOuyang, † JuntangZhuang, † JoyceLee, † YufeiGuo, † WesamManassra, † PrafullaDharwal, † CaseyChu, † YunxinJiao, and Aditya Ramesh. Improving image generation with better captions. 1, 2
- [4] Junsong Chen, Jincheng Yu, Chongjian Ge, Lewei Yao, Enze Xie, Yue Wu, Zhongdao Wang, James T. Kwok, Ping Luo, Huchuan Lu, and Zhenguo Li. Pixart- α : Fast training of diffusion transformer for photorealistic text-to-image synthesis. *ArXiv*, abs/2310.00426, 2023. 1, 2
- [5] Lei Chen, Yuan Meng, Chen Tang, Xinzhu Ma, Jingyan Jiang, Xin Wang, Zhi Wang, and Wenwu Zhu. Q-dit: Accurate post-training quantization for diffusion transformers. *arXiv preprint arXiv:2406.17343*, 2024. 2
- [6] Pengtao Chen, Mingzhu Shen, Peng Ye, Jianjian Cao, Chongjun Tu, Christos-Savvas Bouganis, Yiren Zhao, and Tao Chen. Delta-dit: A training-free acceleration method tailored for diffusion transformers. *arXiv preprint arXiv:2406.01125*, 2024. 2, 3, 4
- [7] Jia Deng, Wei Dong, Richard Socher, Li-Jia Li, Kai Li, and Li Fei-Fei. Imagenet: A large-scale hierarchical image database. In *2009 IEEE conference on computer vision and pattern recognition*, pages 248–255. Ieee, 2009. 4, 5, 7, 2
- [8] Jonathan Ho, Ajay Jain, and Pieter Abbeel. Denoising diffusion probabilistic models. In *Advances in Neural Information Processing Systems 33: Annual Conference on Neural Information Processing Systems 2020, NeurIPS 2020, December 6-12, 2020, virtual*, 2020. 1, 4
- [9] Zhongzhan Huang, Pan Zhou, Shuicheng Yan, and Liang Lin. Scalelong: Towards more stable training of diffusion model via scaling network long skip connection. *Advances in Neural Information Processing Systems*, 36:70376–70401, 2023. 2, 3
- [10] Ziqi Huang, Yinan He, Jiashuo Yu, Fan Zhang, Chenyang Si, Yuming Jiang, Yuanhan Zhang, Tianxing Wu, Qingyang Jin, Nattapol Chanpaisit, Yaohui Wang, Xinyuan Chen, Limin Wang, Dahua Lin, Yu Qiao, and Ziwei Liu. Vbench: Comprehensive benchmark suite for video generative models. In *Proceedings of the IEEE/CVF Conference on Computer Vision and Pattern Recognition (CVPR)*, pages 21807–21818, 2024. 6, 7, 2
- [11] Kumara Kahatapitiya, Haozhe Liu, Sen He, Ding Liu, Menglin Jia, Chenyang Zhang, Michael S Ryoo, and Tian Xie. Adaptive caching for faster video generation with diffusion transformers. *arXiv preprint arXiv:2411.02397*, 2024. 2, 3, 5, 6
- [12] PKU-Yuan Lab and Tuzhan AI etc. Open-sora-plan, 2024. 3
- [13] Senmao Li, Taihang Hu, Fahad Shahbaz Khan, Linxuan Li, Shiqi Yang, Yaxing Wang, Ming-Ming Cheng, and Jian Yang. Faster diffusion: Rethinking the role of unet encoder in diffusion models. *arXiv preprint arXiv:2312.09608*, 2023. 1, 2, 3, 5, 7
- [14] Zhimin Li, Jianwei Zhang, Qin Lin, Jiangfeng Xiong, Yanxin Long, Xincheng Deng, Yingfang Zhang, Xingchao Liu, Minbin Huang, Zedong Xiao, Dayou Chen, Jiajun He, Jiahao Li, Wenyue Li, Chen Zhang, Rongwei Quan, Jianxiang Lu, Jiabin Huang, Xiaoyan Yuan, Xiaoxiao Zheng, Yixuan Li, Jihong Zhang, Chao Zhang, Meng Chen, Jie Liu, Zheng Fang, Weiyang Wang, Jinbao Xue, Yangyu Tao, Jianchen Zhu, Kai Liu, Sihuan Lin, Yifu Sun, Yun Li, Dongdong Wang, Mingtao Chen, Zhichao Hu, Xiao Xiao, Yan Chen, Yuhong Liu, Wei Liu, Di Wang, Yong Yang, Jie Jiang, and Qinglin Lu. Hunyuan-dit: A powerful multi-resolution diffusion transformer with fine-grained chinese understanding, 2024. 2, 3, 7, 4
- [15] Tsung-Yi Lin, Michael Maire, Serge J. Belongie, James Hays, Pietro Perona, Deva Ramanan, Piotr Dollár, and C. Lawrence Zitnick. Microsoft COCO: common objects in context. In *Computer Vision - ECCV 2014 - 13th European Conference, Zurich, Switzerland, September 6-12, 2014, Proceedings, Part V*, pages 740–755. Springer, 2014. 7
- [16] Feng Liu, Shiwei Zhang, Xiaofeng Wang, Yujie Wei, Haonan Qiu, Yuzhong Zhao, Yingya Zhang, Qixiang Ye, and Fang Wan. Timestep embedding tells: It's time to cache for video diffusion model. *arXiv preprint arXiv:2411.19108*, 2024. 2, 3, 5, 6
- [17] Xinyin Ma, Gongfan Fang, and Xinchao Wang. Deepcache: Accelerating diffusion models for free. *2024 IEEE/CVF Conference on Computer Vision and Pattern Recognition (CVPR)*, pages 15762–15772, 2023. 2, 3, 5, 4
- [18] Xin Ma, Yaohui Wang, Gengyun Jia, Xinyuan Chen, Ziwei Liu, Yuan-Fang Li, Cunjian Chen, and Yu Qiao. Latte: Latent diffusion transformer for video generation. *arXiv preprint arXiv:2401.03048*, 2024. 2, 3, 5, 6
- [19] Takeru Miyato, Toshiki Kataoka, Masanori Koyama, and Yuichi Yoshida. Spectral normalization for generative adversarial networks. In *6th International Conference on Learning Representations, ICLR 2018, Vancouver, BC, Canada, April 30 - May 3, 2018, Conference Track Proceedings*. OpenReview.net, 2018. 4
- [20] OpenAI. Sora: Creating video from text. <https://openai.com/sora>, 2024. 2
- [21] Gaurav Parmar, Richard Zhang, and Jun-Yan Zhu. On buggy resizing libraries and surprising subtleties in FID calculation. *CoRR*, abs/2104.11222, 2021. 4, 6
- [22] William Peebles and Saining Xie. Scalable diffusion models with transformers. In *IEEE/CVF International Conference on Computer Vision, ICCV 2023, Paris, France, October 1-6, 2023*, pages 4172–4182. IEEE, 2023. 3, 5, 7, 2
- [23] William S. Peebles and Saining Xie. Scalable diffusion models with transformers. *2023 IEEE/CVF International Conference on Computer Vision, ICCV 2023, Paris, France, October 1-6, 2023*, pages 4172–4182. IEEE, 2023. 3, 5, 7, 2

ence on Computer Vision (ICCV), pages 4172–4182, 2022. 1, 2

[24] Dustin Podell, Zion English, Kyle Lacey, A. Blattmann, Tim Dockhorn, Jonas Muller, Joe Penna, and Robin Rombach. Sdxl: Improving latent diffusion models for high-resolution image synthesis. *ArXiv*, abs/2307.01952, 2023. 1, 2

[25] Adam Polyak, Amit Zohar, Andrew Brown, Andros Tjandra, Animesh Sinha, Ann Lee, Apoorv Vyas, Bowen Shi, Chih-Yao Ma, Ching-Yao Chuang, David Yan, Dhruv Choudhary, Dingkang Wang, Geet Sethi, Guan Pang, Haoyu Ma, Ishan Misra, Ji Hou, Jialiang Wang, Kiran Jagadeesh, Kunpeng Li, Luxin Zhang, Mannat Singh, Mary Williamson, Matt Le, Matthew Yu, Mitesh Kumar Singh, Peizhao Zhang, Peter Vajda, Quentin Duval, Rohit Girdhar, Roshan Sumbaly, Sai Saketh Rambhatla, Sam Tsai, Samaneh Azadi, Samyak Datta, Sanyuan Chen, Sean Bell, Sharadh Ramaswamy, Shelly Sheynin, Siddharth Bhattacharya, Simran Motwani, Tao Xu, Tianhe Li, Tingbo Hou, Wei-Ning Hsu, Xi Yin, Xiaoliang Dai, Yaniv Taigman, Yaqiao Luo, Yen-Cheng Liu, Yi-Chiao Wu, Yue Zhao, Yuval Kirstain, Zecheng He, Zijian He, Albert Pumarola, Ali Thabet, Artsiom Sanakoyeu, Arun Mallya, Baishan Guo, Boris Araya, Breena Kerr, Carleigh Wood, Ce Liu, Cen Peng, Dmitry Vengertsev, Edgar Schonfeld, Elliot Blanchard, Felix Juefei-Xu, Fraylie Nord, Jeff Liang, John Hoffman, Jonas Kohler, Kaolin Fire, Karthik Sivakumar, Lawrence Chen, Licheng Yu, Luya Gao, Markos Georgopoulos, Rashel Moritz, Sara K. Sampson, Shikai Li, Simone Parmeggiani, Steve Fine, Tara Fowler, Vladan Petrovic, and Yuming Du. Movie Gen: A Cast of Media Foundation Models. *arXiv e-prints*, art. arXiv:2410.13720, 2024. 2

[26] Robin Rombach, A. Blattmann, Dominik Lorenz, Patrick Esser, and Björn Ommer. High-resolution image synthesis with latent diffusion models. *2022 IEEE/CVF Conference on Computer Vision and Pattern Recognition (CVPR)*, pages 10674–10685, 2021. 2

[27] Olaf Ronneberger, Philipp Fischer, and Thomas Brox. U-net: Convolutional networks for biomedical image segmentation. *ArXiv*, abs/1505.04597, 2015. 1, 3

[28] Andreas Rössler, Davide Cozzolino, Luisa Verdoliva, Christian Riess, Justus Thies, and Matthias Nießner. Faceforensics: A large-scale video dataset for forgery detection in human faces. *CoRR*, abs/1803.09179, 2018. 5

[29] Axel Sauer, Dominik Lorenz, Andreas Blattmann, and Robin Rombach. Adversarial diffusion distillation. *arXiv preprint arXiv:2311.17042*, 2023. 2

[30] Pratheba Selvaraju, Tianyu Ding, Tianyi Chen, Ilya Zharkov, and Luming Liang. Fora: Fast-forward caching in diffusion transformer acceleration. *arXiv preprint arXiv:2407.01425*, 2024. 1, 2, 4, 5

[31] Aliaksandr Siarohin, Stéphane Lathuilière, Sergey Tulyakov, Elisa Ricci, and Nicu Sebe. First order motion model for image animation. In *Advances in Neural Information Processing Systems 32: Annual Conference on Neural Information Processing Systems 2019, NeurIPS 2019, December 8-14, 2019, Vancouver, BC, Canada*, pages 7135–7145, 2019. 5

[32] Junhyuk So, Jungwon Lee, and Eunhyeok Park. Frdiff: Feature reuse for exquisite zero-shot acceleration of diffusion models. *arXiv preprint arXiv:2312.03517*, 2023. 3

[33] Jiaming Song, Chenlin Meng, and Stefano Ermon. Denoising diffusion implicit models. In *9th International Conference on Learning Representations, ICLR 2021, Virtual Event, Austria, May 3-7, 2021*. OpenReview.net, 2021. 2, 3, 4

[34] Khurram Soomro, Amir Roshan Zamir, and Mubarak Shah. UCF101: A dataset of 101 human actions classes from videos in the wild. *CoRR*, abs/1212.0402, 2012. 5

[35] Zhaochen Su, Linjie Li, Mingyang Song, Yunzhuo Hao, Zhengyuan Yang, Jun Zhang, Guanjie Chen, Jiawei Gu, Juntao Li, Xiaoye Qu, et al. Openthinkimg: Learning to think with images via visual tool reinforcement learning. *arXiv preprint arXiv:2505.08617*, 2025. 3

[36] Zhaochen Su, Peng Xia, Hangyu Guo, Zhenhua Liu, Yan Ma, Xiaoye Qu, Jiaqi Liu, Yanshu Li, Kaide Zeng, Zhengyuan Yang, et al. Thinking with images for multimodal reasoning: Foundations, methods, and future frontiers. *arXiv preprint arXiv:2506.23918*, 2025. 3

[37] Yuchuan Tian, Zhijun Tu, Hanting Chen, Jie Hu, Chao Xu, and Yunhe Wang. U-dits: Downsample tokens in u-shaped diffusion transformers. In *Advances in Neural Information Processing Systems 38: Annual Conference on Neural Information Processing Systems 2024, NeurIPS 2024, Vancouver, BC, Canada, December 10 - 15, 2024*, 2024. 3

[38] Thomas Unterthiner, Sjoerd van Steenkiste, Karol Kurach, Raphaël Marinier, Marcin Michalski, and Sylvain Gelly. Towards accurate generative models of video: A new metric & challenges. *CoRR*, abs/1812.01717, 2018. 6

[39] Yaohui Wang, Xinyuan Chen, Xin Ma, Shangchen Zhou, Ziqi Huang, Yi Wang, Ceyuan Yang, Yinan He, Jiashuo Yu, Peiqing Yang, Yuwei Guo, Tianxing Wu, Chenyang Si, Yuming Jiang, Cunjian Chen, Chen Change Loy, Bo Dai, Dahua Lin, Yu Qiao, and Ziwei Liu. LAVIE: high-quality video generation with cascaded latent diffusion models. *CoRR*, abs/2309.15103, 2023. 6

[40] Zhou Wang and Alan C. Bovik. A universal image quality index. *IEEE Signal Process. Lett.*, 9(3):81–84, 2002. 6

[41] Felix Wimbauer, Bichen Wu, Edgar Schoenfeld, Xiaoliang Dai, Ji Hou, Zijian He, Artsiom Sanakoyeu, Peizhao Zhang, Sam Tsai, Jonas Kohler, et al. Cache me if you can: Accelerating diffusion models through block caching. In *Proceedings of the IEEE/CVF Conference on Computer Vision and Pattern Recognition*, pages 6211–6220, 2024. 3

[42] Wei Xiong, Wenhan Luo, Lin Ma, Wei Liu, and Jiebo Luo. Learning to generate time-lapse videos using multi-stage dynamic generative adversarial networks. In *2018 IEEE Conference on Computer Vision and Pattern Recognition, CVPR 2018, Salt Lake City, UT, USA, June 18-22, 2018*, pages 2364–2373. Computer Vision Foundation / IEEE Computer Society, 2018. 5

[43] Zhuoyi Yang, Jiayan Teng, Wendi Zheng, Ming Ding, Shiyu Huang, Jiazheng Xu, Yuanming Yang, Wenyi Hong, Xiaohan Zhang, Guanyu Feng, et al. Cogvideox: Text-to-video diffusion models with an expert transformer. *arXiv preprint arXiv:2408.06072*, 2024. 3

[44] Jingfeng Yao, Cheng Wang, Wenyu Liu, and Xinggang Wang. Fasterdit: Towards faster diffusion transformers training without architecture modification. *Advances in Neural Information Processing Systems*, 37:56166–56189, 2025. 2, 4

[45] Tianwei Yin, Michaël Gharbi, Richard Zhang, Eli Shechtman, Fredo Durand, William T Freeman, and Taesung Park. One-step diffusion with distribution matching distillation. In *Proceedings of the IEEE/CVF Conference on Computer Vision and Pattern Recognition*, pages 6613–6623, 2024. [2](#)

[46] Yuichi Yoshida and Takeru Miyato. Spectral norm regularization for improving the generalizability of deep learning. *CoRR*, abs/1705.10941, 2017. [4](#)

[47] Sihyun Yu, Jihoon Tack, Sangwoo Mo, Hyunsu Kim, Junho Kim, Jung-Woo Ha, and Jinwoo Shin. Generating videos with dynamics-aware implicit generative adversarial networks. In *International Conference on Learning Representations*, 2022. [6](#)

[48] Richard Zhang, Phillip Isola, Alexei A Efros, Eli Shechtman, and Oliver Wang. The unreasonable effectiveness of deep features as a perceptual metric. In *Proceedings of the IEEE conference on computer vision and pattern recognition*, pages 586–595, 2018. [6](#)

[49] Wentian Zhang, Haozhe Liu, Jinheng Xie, Francesco Faccio, Mike Zheng Shou, and Jürgen Schmidhuber. Cross-attention makes inference cumbersome in text-to-image diffusion models. *CoRR*, abs/2404.02747, 2024. [2](#), [7](#)

[50] Wentian Zhang, Haozhe Liu, Jinheng Xie, Francesco Faccio, Mike Zheng Shou, and Jürgen Schmidhuber. Cross-attention makes inference cumbersome in text-to-image diffusion models. *arXiv preprint arXiv:2404.02747*, 2024. [3](#), [5](#)

[51] Yiming Zhang, Zhening Xing, Yanhong Zeng, Youqing Fang, and Kai Chen. Pia: Your personalized image animator via plug-and-play modules in text-to-image models. In *Proceedings of the IEEE/CVF Conference on Computer Vision and Pattern Recognition*, pages 7747–7756, 2024. [1](#)

[52] Wangbo Zhao, Yizeng Han, Jiasheng Tang, Kai Wang, Yibing Song, Gao Huang, Fan Wang, and Yang You. Dynamic diffusion transformer. *arXiv preprint arXiv:2410.03456*, 2024. [2](#), [3](#)

[53] Xuanlei Zhao, Xiaolong Jin, Kai Wang, and Yang You. Real-time video generation with pyramid attention broadcast, 2024. [2](#), [3](#), [6](#), [7](#), [8](#), [4](#)

[54] Zangwei Zheng, Xiangyu Peng, Tianji Yang, Chenhui Shen, Shenggui Li, Hongxin Liu, Yukun Zhou, Tianyi Li, and Yang You. Open-sora: Democratizing efficient video production for all, 2024. [3](#), [7](#)

Towards Stabilized and Efficient Diffusion Transformers through Long-Skip-Connections with Spectral Constraints

Supplementary Material

6. Limitations

Despite achieving significant speedups, Skip-DiT inherits limitations from its DiT foundation, including high computational demands, reliance on large-scale training data, and quadratic complexity that hinders high-resolution generation. Furthermore, Skip-DiT introduces a marginal parameter overhead (5.5% for class-to-image, 3.5% for text-to-video) and extra GPU memory (scales with the batch size \mathcal{N}), requiring an additional $\mathcal{N} \times 0.37\%$ for the class-to-image model and $\mathcal{N} \times 4.55\%$ for the text-to-video model. These models remain feasible for deployment with proper \mathcal{N} .

7. Supplementary Experiments

Analysis of Block Selection for Caching To identify the optimal block for caching, we analyze the feature similarity across timesteps in the final three blocks of Latte-T2V (Table 7). Our analysis reveals that caching at block 27, the last DiT block, yields the best performance. This block, which is connected to block 0 via the primary Long Skip Connection (LSC), not only exhibits maximum feature similarity but also enables the highest speedup. These results demonstrate the superior caching efficiency achieved by Skip-DiT.

Table 7. Connection selection for caching in the text-to-video task. The best metrics are emphasized in **bold**.

| LSC | Cached | Similarity(%) \uparrow | VBench(%) \uparrow | PSNR \uparrow | LPIPS \downarrow | SSIM \uparrow |
|-----|--------|--------------------------|----------------------|-----------------|--------------------|-----------------|
| 0 | [1,26] | 99.88 | 75.51 | 29.52 | 0.06 | 0.89 |
| 1 | [2,25] | 99.86 | 75.44 | 29.65 | 0.06 | 0.89 |
| 2 | [3,24] | 99.66 | 75.49 | 29.44 | 0.06 | 0.88 |

Comparison in Few-Step Generation We benchmarked Skip-DiT against a vanilla DiT in a few-step text-to-video generation scenario, using a 5 and 10-step DDIM scheduler instead of the standard 50 steps. As shown in Table 8, while the vanilla DiT holds a slight advantage in the SSIM metric, Skip-DiT achieves superior visual quality and semantic consistency. These results again validate the balanced and robust performance of our architecture, even in a highly accelerated, few-step setting.

8. Detailed Proof of Theorems

Consider an ideal denoising diffusion transformer M with L identical blocks, where the denoising capability induces the following fundamental properties:

Table 8. Text-to-video generation performance under the few-step scenario. The best metrics are emphasized in **bold**.

| NFE | Model | Δ VBench(%) | PSNR \uparrow | LPIPS \downarrow | SSIM \uparrow |
|----------|-----------------|-------------------------------------|-----------------|--------------------|-----------------|
| 10 steps | Latte | $\downarrow 1.73$ | 15.96 | 0.47 | 0.61 |
| | Skip-DiT | $\downarrow 0.94$ | 16.18 | 0.43 | 0.59 |
| 5 steps | Latte | $\downarrow 9.40$ | 12.94 | 0.73 | 0.53 |
| | Skip-DiT | $\downarrow 8.55$ | 13.17 | 0.69 | 0.50 |

- *Noise Reduction Invariance*: Each transformer block \mathcal{T}_l strictly reduces noise magnitude of input h . This directly implies the Jacobian spectral norm (σ_{\max}) constraint:

$$\sigma_{\max} \left(\frac{\partial \mathcal{T}_l}{\partial h} \right) \triangleq \gamma_l < 1 \quad (9)$$

- *Transformer Blocks Homogeneity*: Identical noise reduction ratio across layers $\gamma_l = \gamma, \forall l \in \{1, \dots, L\}$. Thus, the complete model satisfies

$$\sigma_{\max}(M) = \prod_{l=1}^L \gamma = \gamma^L \ll 1 \quad (10)$$

8.1. Theorem1

The spectral norm of the Jacobian matrix of DiT with Long-Skip-Connections is controlled tighter than that of Vanilla DiT M , making the Skip-DiT model more robust, numerically stable, and capable of converging faster.

Proof. Define layer transformations for $L/2 < l \leq L$ and their Jacobian matrices, where \mathcal{T} denotes the Transformer block and $0 < \alpha < 1$:

$$h_{l+1}^{\text{vanilla}} = \mathcal{T}(h_l^{\text{vanilla}}), h_{l+1}^{\text{skip}} = (1 - \alpha) \cdot \mathcal{T}(h_l^{\text{skip}}) + \alpha \cdot h_{L-l}^{\text{skip}}.$$

The corresponding Jacobian matrices J are:

$$J_l^{\text{vanilla}} = \frac{\partial \mathcal{T}(h_l)}{\partial h_l}, J_l^{\text{skip}} = (1 - \alpha) \cdot \frac{\partial \mathcal{T}(h_l)}{\partial h_l} + \alpha \cdot \frac{\partial h_{L-l}}{\partial h_l}.$$

Applying subadditivity and submultiplicativity of spectral norms σ_{\max} :

$$\sigma_{\max}(J_l^{\text{skip}}) \leq (1 - \alpha)\gamma + \alpha\gamma^{2l-L}. \quad (11)$$

Given $\gamma < 1$ and $2l - L \geq 1$ for $l > L/2$, we establish the layer-wise bound:

$$\sigma_{\max}(J_l^{\text{skip}}) < \gamma = \sigma_{\max}(J_l^{\text{vanilla}}). \quad (12)$$

For the full model Jacobian $J = \prod_{l=1}^L J_l$, the spectral norms satisfy:

$$\begin{aligned}\sigma_{\max}(J^{\text{skip}}) &\leq \prod_{l=0}^{L-1} [(1-\alpha)\gamma + \alpha\gamma^{2l-L}] \\ &< \prod_{l=0}^{L-1} \gamma = \gamma^L = \sigma_{\max}(J^{\text{vanilla}}).\end{aligned}\quad (13)$$

This spectral radius reduction attenuates perturbation growth through $\|\delta h_L\| \leq (\sigma_{\max}(J))^L \|\delta h_0\|$, stabilizes gradient flow via $\|\nabla_{\theta} \mathcal{L}\| \leq \sigma_{\max}(J) \|\nabla_{h_L} \mathcal{L}\|$, and improves the Lipschitz constant $\text{Lip}(M_{\text{skip}}) < \text{Lip}(M_{\text{vanilla}})$. \square

8.2. Theorem2

Under feature reuse with interval τ , Skip-DiT achieves tighter perturbation bounds than Vanilla DiT, enabling larger allowable reuse intervals while maintaining error tolerance ϵ_{\max}

Proof. Let h_t be the reused feature with error ϵ_t , δ the perturbation bound per step, x the input, and θ the model parameters. Through the differential mean-value theorem and error propagation:

$$\|f(x; \theta + \Delta\theta) - f(x; \theta)\| \leq \sup_{\theta'} \left\| \frac{\partial f}{\partial \theta} \right\| \|\Delta\theta\| \triangleq \delta \quad (14)$$

$$\epsilon_{t+1} = \|h_{t+1} - h_t\| \leq \text{Lip}(M)\epsilon_t + \delta \quad (15)$$

From Theorem 1, the Lipschitz constants satisfy:

$$\text{Lip}(M_{\text{skip}}) = \sigma_{\max}(J^{\text{skip}}) < \gamma^L = \text{Lip}(M_{\text{vanilla}}) \quad (16)$$

The perturbation bounds inherit:

$$\delta_{\text{skip}} = C_{\text{skip}} \|\Delta\theta\| < C_{\text{vanilla}} \|\Delta\theta\| = \delta_{\text{vanilla}} \quad (17)$$

where C bounds the parameter-to-output Jacobian.

$$\begin{aligned}\left\| \frac{\partial f_{\text{skip}}}{\partial \theta} \right\| &= \left\| \prod_{l=1}^L \frac{\partial h_l}{\partial \theta} \right\| \leq \prod_{l=1}^L \left\| \frac{\partial h_l}{\partial \theta} \right\| \\ &= \prod_{l=1}^L [(1-\alpha)\gamma + \alpha\gamma^{2l-L}] \cdot C_{\text{base}} \\ &< \prod_{l=1}^L \gamma \cdot C_{\text{base}} = C_{\text{vanilla}}\end{aligned}$$

For T -step feature reuse, cumulative error develops as:

$$\epsilon_T \leq \frac{\text{Lip}(M)^T - 1}{\text{Lip}(M) - 1} \delta \quad (18)$$

Given $\sigma_{\max}(J^{\text{skip}}) < \gamma^L$ and $\delta_{\text{skip}} < \delta_{\text{vanilla}}$, the maximal interval τ satisfies:

$$\frac{\sigma_{\max}(J^{\text{skip}})^{\tau} - 1}{\sigma_{\max}(J^{\text{skip}}) - 1} \delta_{\text{skip}} = \frac{\gamma^{L\tau} - 1}{\gamma^L - 1} \delta_{\text{vanilla}} = \epsilon_{\max} \quad (19)$$

Solving equation 19 yields $\tau_{\text{skip}} > \tau_{\text{vanilla}}$ under identical ϵ_{\max} , proving Skip-DiT permits larger reuse intervals. \square

Table 9. Comparison of training efficiency between DiT-XL and Skip-DiT. Images are generated with a 250-step DDPM solver. The term cfg refers to classifier-free guidance scales, where metrics for $cfg=1.0$ are computed without classifier-free guidance. The best metrics are highlighted in **bold**. Skip-DiT significantly exceeds DiT-XL/2 with much less training steps.

| Model | Steps | FID \downarrow | sFID \downarrow | IS \uparrow | Precision \uparrow | Recall \uparrow |
|----------|-------|------------------|-------------------|---------------|----------------------|-------------------|
| DiT-XL/2 | 7000k | 9.49 | 7.17 | 122.49 | 0.67 | 0.68 |
| | 400k | 13.46 | 5.83 | 87.45 | 0.67 | 0.63 |
| | 800k | 10.13 | 5.87 | 108.28 | 0.68 | 0.65 |
| | 1600k | 9.07 | 6.26 | 119.38 | 0.68 | 0.67 |
| | 2200k | 8.59 | 6.41 | 124.74 | 0.68 | 0.67 |
| | 2500k | 8.41 | 6.30 | 125.16 | 0.68 | 0.67 |
| | 2900k | 8.37 | 6.50 | 127.63 | 0.68 | 0.68 |

9. Class-to-image Generation Experiments

Peebles and Xie [22] proposed the first diffusion model based on the transformer architecture, and it outperforms all prior diffusion models on the class conditional ImageNet [7] 512×512 and 256×256 benchmarks. We add skip connections to its largest model, DiT-XL, to get Skip-DiT. We train Skip-DiT on class conditional ImageNet with resolution 256×256 from scratch with completely the same experimental settings as DiT-XL, and far exceeds DiT-XL with only around 38% of its training cost.

Training of Skip-DiT We add long-skip-connections in DiT-XL and train Skip-DiT for 2.9M steps on 8 A100 GPUs, compared to 7M steps for DiT-XL, which also uses 8 A100 GPUs. The datasets and other training settings remain identical to those used for DiT-XL, and we utilize the official training code of DiT-XL[†]. The performance comparison is presented in Table 9, which demonstrates that Skip-DiT significantly outperforms DiT-XL while requiring only 23% of its training steps (1.6M vs. 7M), highlighting the training efficiency and effectiveness of Skip-DiT.

Accelerating Evaluation We evaluate Skip-DiT and compare its performance against two other caching methods: Δ -DiT and FORA. As shown in Table 10, Skip-DiT achieves a 1.46× speedup with only a minimal FID loss of 0.02 when the classifier-free guidance scale is set to 1.5, compared to the 7–8× larger losses observed with Δ -DiT and FORA. Moreover, even with a 1.9× acceleration, Skip-DiT performs better than the other caching methods. These findings further confirm the effectiveness of Skip-DiT for class-to-image tasks.

10. Evaluation Details

VBench [10] is a novel evaluation framework for video generation models. It breaks down video generation assess-

[†]<https://github.com/facebookresearch/DiT>

Table 10. Class-to-image generation performance. The definition of the cache step n follows that in Table 4. Images are generated with a 250-step DDPM solver. Speedups are calculated on an H100 GPU with a sample batch size of 8. $n = i$ indicates caching the high-level features in x_t for reuse during the inference of $x_{t-1}, x_{t-2}, \dots, x_{t-n+1}$. The term cfg refers to classifier-free guidance scales, where metrics for $cfg=1.0$ are computed without classifier-free guidance. We highlight baseline DiT models (without caching) in grey and the best metrics in **bold**.

| Methods | FID ↓ | sFID ↓ | IS ↑ | Precision% | Recall% | Speedup |
|--------------------------------|-------------|-------------|---------------|--------------|--------------|---------------|
| <i>cfg=1.5</i> | | | | | | |
| DiT-XL | 2.30 | 4.71 | 276.26 | 82.68 | 57.65 | 1.00× |
| FORA | 2.45 | 5.44 | 265.94 | 81.21 | 58.36 | 1.57× |
| Delta-DiT | 2.47 | 5.61 | 265.33 | 81.05 | 58.83 | 1.45× |
| Faster-Diff | 4.96 | 10.19 | 223.21 | 75.21 | 59.28 | 1.42× |
| Skip-DiT with Cached Inference | | | | | | |
| Skip-DiT | 2.29 | 4.58 | 281.81 | 82.88 | 57.53 | 1.00× |
| $n = 2$ | 2.31 | 4.76 | 277.51 | 82.52 | 58.06 | 1.46× |
| $n = 3$ | 2.40 | 4.98 | 272.05 | 82.14 | 57.86 | 1.73× |
| $n = 4$ | 2.54 | 5.31 | 267.34 | 81.60 | 58.31 | 1.93 × |
| <i>cfg=1.0</i> | | | | | | |
| DiT-XL | 9.49 | 7.17 | 122.49 | 66.66 | 67.69 | 1.00× |
| FORA | 11.72 | 9.27 | 113.01 | 64.46 | 67.69 | 1.53× |
| Delta-DiT | 12.03 | 9.68 | 111.86 | 64.57 | 67.53 | 1.42× |
| Faster-Diff | 22.98 | 18.09 | 80.41 | 56.53 | 67.41 | 1.42× |
| Skip-DiT with Cached Inference | | | | | | |
| Skip-DiT | 8.37 | 6.50 | 127.63 | 68.06 | 67.89 | 1.00× |
| $n = 2$ | 9.25 | 7.09 | 123.57 | 67.32 | 67.40 | 1.46× |
| $n = 3$ | 10.18 | 7.72 | 119.60 | 66.53 | 67.84 | 1.71× |
| $n = 4$ | 11.37 | 8.49 | 116.01 | 65.73 | 67.32 | 1.92 × |

ment to 16 dimensions from video quality and condition consistency: subject consistency, background consistency, temporal flickering, motion smoothness, dynamic degree, aesthetic quality, imaging quality, object class, multiple objects, human action, color, spatial relationship, scene, temporal style, appearance style, overall consistency.

Peak Signal-to-Noise Ratio (PSNR) measures generated visual content quality by comparing a processed version \mathbf{v} to the original reference \mathbf{v}_r by:

$$\text{PSNR} = 10 \times \log_{10} \left(\frac{R^2}{\text{MSE}(\mathbf{v}, \mathbf{v}_r)} \right) \quad (20)$$

where R is the maximum possible pixel value, and $\text{MSE}(\cdot, \cdot)$ calculates the Mean Squared Error between original and processed images or videos. Higher PSNR indicates better reconstruction quality. However, PSNR does not always correlate with human perception and is sensitive to pixel-level changes.

Structural Similarity Index Measure (SSIM) is a perceptual metric that evaluates image quality by considering luminance, contrast, and structure:

$$\text{SSIM} = [l(\mathbf{v}, \mathbf{v}_r)]^\alpha \cdot [c(\mathbf{v}, \mathbf{v}_r)]^\beta \cdot [s(\mathbf{v}, \mathbf{v}_r)]^\gamma \quad (21)$$

where α, β, γ are weights for luminance, contrast, and structure quality, where luminance comparison is $l(x, y) = \frac{2\mu_v\mu_{v_r} + C_1}{\mu_v^2 + \mu_{v_r}^2 + C_1}$, contrast comparison is $c(x, y) = \frac{2\sigma_v\sigma_{v_r} + C_2}{\sigma_v^2 + \sigma_{v_r}^2 + C_2}$, and structure comparison is $s(x, y) = \frac{\sigma_{xy} + C_3}{\sigma_v\sigma_{v_r} + C_3}$, with C denoting numerical stability coefficients. SSIM scores range from -1 to 1, where 1 means identical visual content.

Learned Perceptual Image Patch Similarity (LPIPS) is a deep learning-based metric that measures perceptual similarity using L2-Norm of visual features $v \in \mathbb{R}^{H \times W \times C}$ extracted from pretrained CNN $\mathcal{F}(\cdot)$. LPIPS captures semantic similarities and is therefore more robust to small geometric transformations than PSNR and SSIM.

$$\text{LPIPS} = \frac{1}{HW} \sum_{h,w} \|\mathcal{F}(v_r) - \mathcal{F}(v)\|_2^2 \quad (22)$$

Fréchet Inception Distance (FID) and Fréchet Video Distance (FVD) FID measures the quality and diversity of generated images by computing distance between feature distributions of reference $\mathcal{N}(\mu_r, \Sigma_r)$ and generated images $\mathcal{N}(\mu, \Sigma)$ using inception architecture CNNs, where μ, Σ are mean and covariance of features.

$$\text{FID} = \|\mu_r - \mu\|^2 + \text{Tr}(\Sigma_r + \Sigma - 2(\Sigma_r \Sigma)^{1/2}) \quad (23)$$

FVD is a video extension of FID. Lower FID and FVD indicate higher generation quality.

Table 11. Comparison of our caching method with the faster sampler DDIM. Skip-Cache is evaluated with a 250-steps DDPM and compared to the DDIM sampler under similar throughput. Baseline DiT models (without caching) are highlighted in grey, and the best metrics are indicated in **bold**. Notably, DDIM outperforms the 250-step DDPM in the UCF101 task for both Latte and Skip-DiT. Skip-Cache denotes Skip-DiT with cached inference.

| Method | UCF101 | | FFS | | Sky | | Taichi | |
|-------------------------|---------------|--------------|--------------|-------------|--------------|--------------|---------------|--------------|
| | FVD ↓ | FID ↓ | FVD ↓ | FID ↓ | FVD ↓ | FID ↓ | FVD ↓ | FID ↓ |
| Latte | 165.04 | 23.75 | 28.88 | 5.36 | 49.46 | 11.51 | 166.84 | 11.57 |
| Skip-DiT | 173.70 | 22.95 | 20.62 | 4.32 | 49.22 | 12.05 | 163.03 | 13.55 |
| Skip-DiT _{n=2} | 165.60 | 22.73 | 23.55 | 4.49 | 51.13 | 12.66 | 167.54 | 13.89 |
| DDIM+Skip-DiT | 134.22 | 24.60 | 37.28 | 6.48 | 86.39 | 13.67 | 343.97 | 21.01 |
| DDIM+Latte | 146.78 | 23.06 | 39.10 | 6.47 | 78.38 | 13.73 | 321.97 | 21.86 |
| Skip-DiT _{n=3} | 169.37 | 22.47 | 26.76 | 4.75 | 54.17 | 13.11 | 179.43 | 14.53 |
| DDIM+Skip-DiT | 139.52 | 24.71 | 39.20 | 6.49 | 90.62 | 13.80 | 328.47 | 21.33 |
| DDIM+Latte | 148.46 | 23.41 | 41.00 | 6.54 | 74.39 | 14.20 | 327.22 | 22.96 |

11. Scheduler Selection for text-to-video Tasks

For the text-to-video generation task, all the videos generated for evaluation are sampled with 50 steps DDIM [33], which is the default setting used in Latte. In the class-to-video

generation tasks, vanilla Latte uses 250-step DDPM [8] as the default solver for class-to-video tasks, which we adopt for all tasks except UCF101. For UCF101, we employ 50-step DDIM [33], as it outperforms 250-step DDPM on both Latte and Skip-DiT. Table 11 highlights this phenomenon, showing our methods consistently outperform DDPM-250 under comparable throughput, except for UCF101, where DDIM performs better than 250 steps DDPM. In the text-to-image task, we choose 50-step DDIM for sampling, and for the class-to-image task, we choose 250-steps DDPM.

12. Implementation of Other Caching Methods

DeepCache DeepCache [17] is a training-free caching method designed for U-Net-based diffusion models, leveraging the inherent temporal redundancy in sequential denoising steps. It utilizes the skip connections of the U-Net to reuse high-level features while updating low-level features efficiently. Skip-DiT shares significant similarities with DeepCache but extends the method to DiT models. Specifically, we upgrade traditional DiT models to Skip-DiT and cache them using Skip-DiT. In the work of DeepCache, two key caching decisions are introduced: (1) N : the number of steps for reusing cached high-level features. Cached features are computed once and reused for the next $N-1$ steps. (2) The layer at which caching is performed. For instance, caching at the first layer ensures that only the first and last layers of the U-Net are recomputed. In Skip-DiT, we adopt these two caching strategies and additionally account for the timesteps to cache, addressing the greater complexity of DiT models compared to U-Net-based diffusion models. For all tasks except the class-to-image task, caching is performed at the first layer, whereas for the class-to-image task, it is applied at the third layer.

Δ -DiT Δ -DiT [6] is a training-free caching method designed for image-generating DiT models. Instead of caching the feature maps directly, it uses the offsets of features as cache objects to preserve input information. This approach is based on the observation that the front blocks of DiT are responsible for generating the image outlines, while the rear blocks focus on finer details. A hyperparameter b is introduced to denote the boundary between the outline and detail generation stages. When $t \leq b$, Δ -Cache is applied to the rear blocks; when $t > b$, it is applied to the front blocks. The number of cached blocks is represented by N_c . While this caching method was initially designed for image generation tasks, we extend it to video generation tasks. In video generation, we observe significant degradation in performance when caching the rear blocks, so we restrict caching to the front blocks during the outline generation stage. For Hunyuan-DiT [14], we cache the middle blocks due to the U-shaped transformer architecture. Detailed configurations are provided in Table 12.

Table 12. Configuration details for Δ -Cache in different models and tasks. $t2v$ denotes text-to-video, $c2v$ denotes class-to-video, $t2i$ denotes text-to-image, and $c2i$ denotes class-to-image.

| Δ -DiT | Task | Diffusion steps | b | All layers | N_c |
|---------------|-------|-----------------|-----|------------|-------|
| Latte | $t2v$ | 50 | 12 | 28 | 21 |
| Latte | $c2v$ | 250 | 60 | 14 | 10 |
| Hunyuan | $t2i$ | 50 | 12 | 28 | 18 |
| DiT-XL/2 | $c2i$ | 250 | 60 | 28 | 21 |

PAB PAB (Pyramid Attention Broadcast) [53] is one of the most promising caching methods designed for real-time video generation. The method leverages the observation that attention differences during the diffusion process follow a U-shaped pattern, broadcasting attention outputs to subsequent steps in a pyramid-like manner. Different broadcast ranges are set for three types of attention—spatial, temporal, and cross-attention—based on their respective differences. $PAB_{\alpha\beta\gamma}$ denotes the broadcast ranges for spatial (α), temporal (β), and cross (γ) attentions.

In this work, we use the official implementation of PAB for text-to-video tasks on Latte and adapt the caching method to other tasks in-house. For the class-to-video task, where cross-attention is absent, $PAB_{\alpha\beta}$ refers to the broadcast ranges of spatial (α) and temporal (β) attentions. In the text-to-image task, which lacks temporal attention, $PAB_{\alpha\beta}$ instead denotes the broadcast ranges of spatial (α) and cross (β) attentions. We do not apply PAB to the class-to-image task, as it involves only spatial attention.

Table 13. Configuration details for T-GATE in different settings. $t2v$ denotes text-to-video, $t2i$ denotes text-to-image.

| T-GATE | Task | Diffusion steps | m | k |
|-------------|-------|-----------------|-----|-----|
| Latte | $t2v$ | 50 | 20 | 2 |
| Hunyuan-DiT | $t2i$ | 50 | 20 | 2 |

T-Gates T-Gates divide the diffusion process into two phases: (1) the Semantics-Planning Phase and (2) the Fidelity-Improving Phase. In the first phase, self-attention is computed and reused every k step. In the second phase, cross-attention is cached using a caching mechanism. The hyperparameter m determines the boundary between these two phases. For our implementation, we use the same hyperparameters as PAB [53]. Detailed configurations are provided in Table 13.

FORA FORA (Fast-Forward Caching) [30] stores and reuses intermediate outputs from attention and MLP layers across denoising steps. However, in the original FORA paper, features are cached in advance before the diffusion process. We do not adopt this approach, as it is a highly time-consuming process. Instead, in this work, we skip the “Initialization” step in FORA and calculate the features dynamically during the diffusion process.

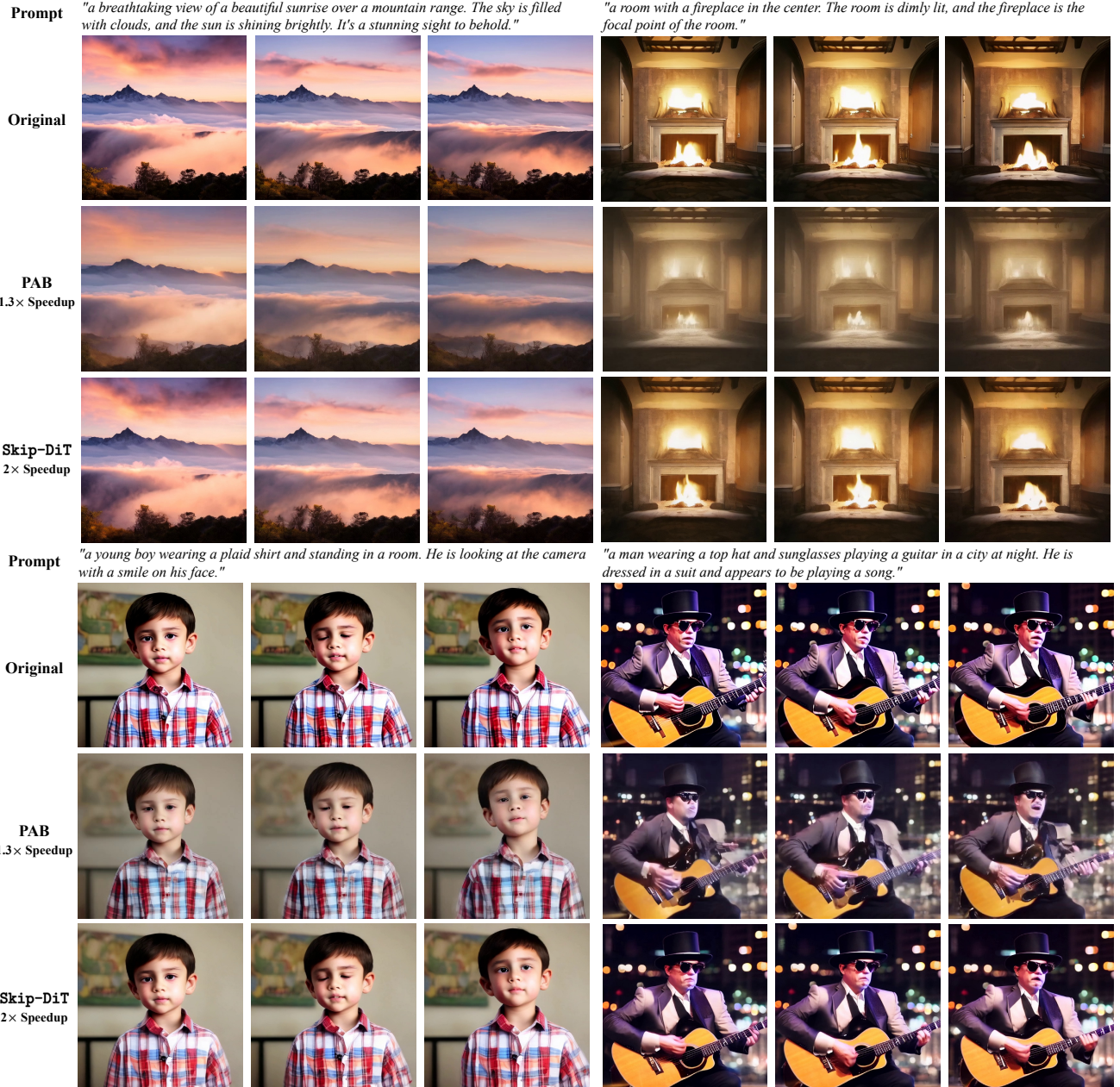


Figure 6. Qualitative results of text-to-video generation. We present Skip-DiT, PAB₄₆₉, and the original model. The frames are randomly sampled from the generated video.

AdaCache AdaCache [11] identifies the feature sample-variance in the DiT, and proposes to predict the feature similarity of the current timestep to decide whether to cache. The codebook for Latte, which records the threshold is not released. We provide a version of codebook which almost reproduce the performance in the paper. The codebook is as follows: $\{0.08 : 3, 0.10 : 2, 0.12 : 1\}$

TeaCache Same as AdaCache, TeaCache[16] also discovers the feature instability in DiT. Different from AdaCache, TeaCache finds the relationship between input and output similarity and employ high-order polynomial functions to predict the similarity of the current timestep. We use the official codebase of it and choose the slow-caching strategy to evaluate its upper-bound.

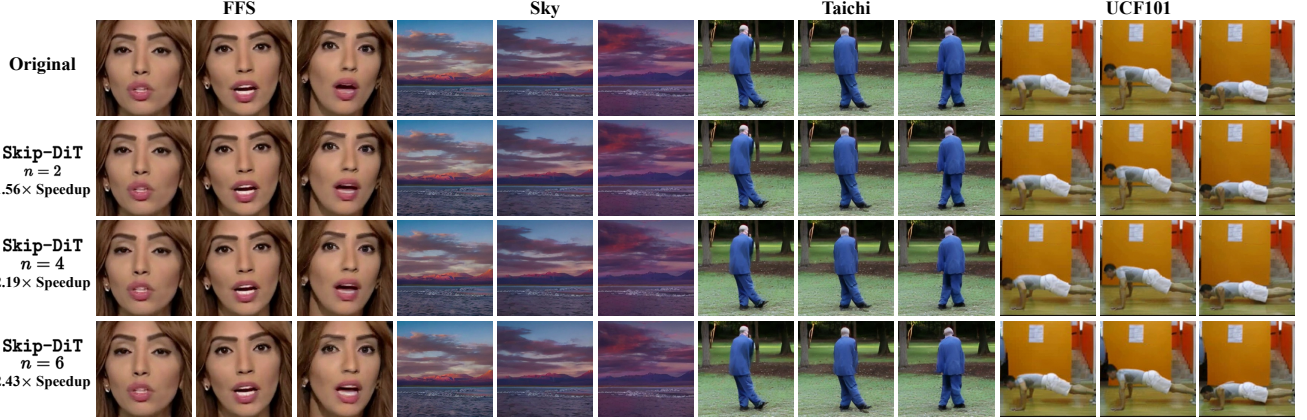


Figure 7. Qualitative results of class-to-video generation. We present the original video generation model and Skip-DiT with different caching steps n . The frames are randomly sampled from the generated video.

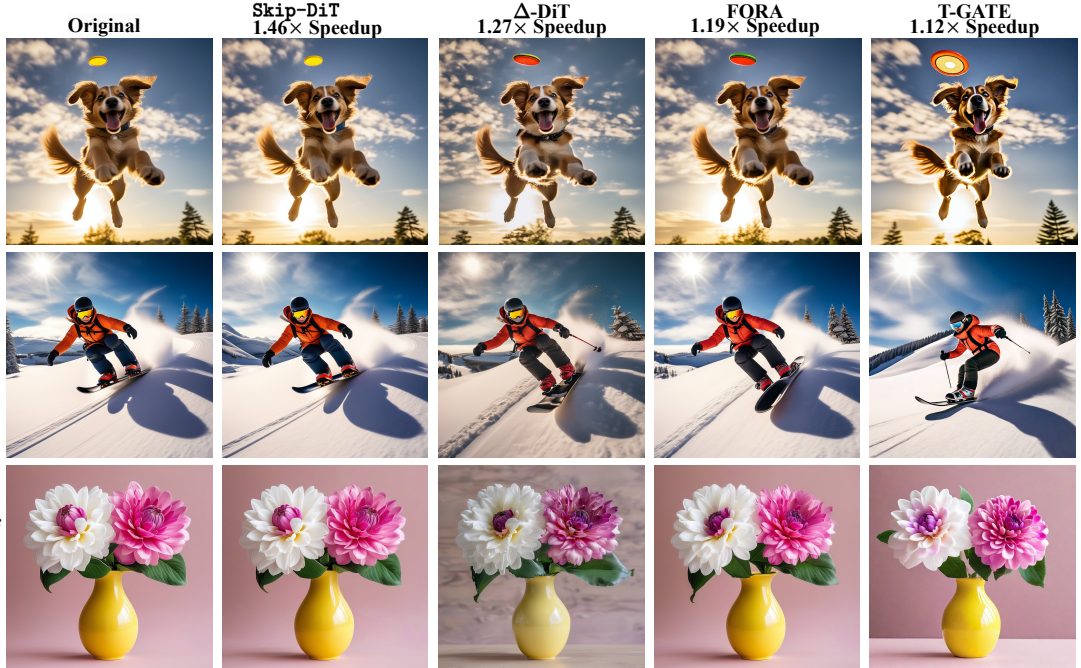


Figure 8. Qualitative results of text-to-image generation. We present Skip-DiT, Δ -DiT, FORA, T-GATE, and the original model.

13. Case Study

Video Generation In Figure 6, we showcase the generated video frames from text prompts with Skip-DiT, PAB, and comparing them to the original model. From generating portraits to scenery, Skip-DiT with caching consistently demonstrates better visual fidelity along with faster generation speeds. Figure 7 presents class-to-video generation examples with Skip-DiT with varying caching steps $\in \{2, 4, 6\}$. By comparing the output of Skip-DiT with cache to standard output, we see Skip-DiT maintains good generation quality across different caching steps.

Image Generation Figure 8 compares qualitative results of Skip-DiT compared to other caching-based acceleration methods (Δ -DiT, FORA, T-GATE) on Hunyuan-DiT. In Figure 9, Skip-DiT show distinct edges in higher speedup and similarity to the original generation, while other baselines exist with different degrees of change in details such as color, texture, and posture. Similarly, we present Skip-DiT with varying caching steps in Figure 9, showing that with more steps cached, it still maintains high fidelity to the original generation.



Figure 9. Qualitative results of class-to-image generation. We present the original image generation model and Skip-DiT with different caching steps n .